Heliyon 8 (2022) e10341

Contents lists available at ScienceDirect

Heliyon

journal homepage: www.cell.com/heliyon

Research article

Prevention of inorganic arsenic induced squamous cell carcinoma of the skin in Swiss albino mice by black tea through epigenetic modulation

Archismaan Ghosh [a], Ansuman Lahiri [b], Sutapa Mukherjee [a], Madhumita Roy [a], Amitava Datta [c,*]

[a] Department of Environmental Carcinogenesis & Toxicology, Chittaranjan National Cancer Institute, 37, S P Mukherjee Road, Kolkata 700026, India
[b] Department of Biophysics, Molecular Biology & Bioinformatics, University of Calcutta, 92, APC Road, Kolkata 700009, India
[c] Department of Computer Science and Software Engineering, University of Western Australia, Perth, WA 6009, Australia

ARTICLE INFO

Keywords:
Inorganic arsenic
Squamous cell carcinoma
Methyltransferases
Demethylases
Acetyltransferases
Black tea extract
JARID1B

ABSTRACT

Consumption of inorganic Arsenic (iAs) above the safe level may lead to many diseases including cancers of skin. It is known that carcinogenicity of iAs is mediated through generation of excessive reactive oxygen species and polyphenols present in black tea extract (BTE) ameliorate the deleterious effect. Epigenetics also plays vital roles in carcinogenesis. The aim of this paper is to study the influence of iAs on epigenetics and the modulatory effect of BTE.

Male Swiss albino mice were divided into three groups, (i) control, (ii) iAs-administered and (iii) iAs + BTE administered. Group (ii) developed invasive squamous cell carcinoma (SCC) of the skin after 330 days, while only hyperplasic and dysplastic changes were observed in group (iii). Expression levels of histone methylation, acetylation marks and several histone methylases, demethylases and acetylases due to iAs were studied; most aberrant expression levels due to iAs were modulated by BTE. JARID1B, a histone demethylase implicated as one of the markers in SCC and a therapeutic target gets upregulated by iAs, but is not influenced by BTE. However, SCC is prevented by BTE. Upregulation of JARID1B by iAs represses H3K4me3; BTE upregulates H3K4me3 without influencing JARID1B expression level. It is known that theaflavin compounds in BTE are transported to the nucleus and interact with histone proteins. in-silico findings in this paper hint that theaflavin compounds present in BTE are very good inhibitors of JARID1B and BTE inhibits its demethylating activity. BTE reverses the epigenetic alterations caused by iAs, thus aids in prevention of SCC.

1. Introduction

Genetic mutation, epigenetic modulation and environmental factors contribute to carcinogenesis. Chronic exposure to inorganic arsenic (iAs), a class I carcinogen declared by IARC [1] beyond the safe level (10 μg/L, as set by WHO) [1], leads to numerous diseases including cancers of the skin, bladder, kidney and liver [2]. Globally iAs contaminated drinking water is a major health hazard. Air borne particulate matter released from several industries also adds to the risk [3]. Arsenic mediates its carcinogenicity by excessive generation of reactive oxygen species (ROS) [2]. Metabolism of inorganic arsenic (iAs) utilises S-adenosyl methionine (SAM), whose depletion occurs due to chronic exposure to iAs, altering global methylation pattern of DNA and gene expression [4]. iAs is also known to induce different types of epigenetic modulations, and the present study focuses on post-translational histone modifications (PTM) including histone methylation, demethylation and acetylation. The main contributions of this study are two-fold. The carcinogenic effect of iAs on squamous cell carcinoma (SCC) due to PTM and the alleviation of these effects by black tea extract (BTE) have been studied extensively *in vivo* in the mouse model. The effects of iAs on several of these methylases and demethylases have not been reported before to the best of our knowledge. This paper also establishes the potential of theaflavin compounds (present in BTE) as inhibitors of JARID1B, a di- and tri-demethylase of H3K4 through extensive in silico studies.

Antioxidants mitigate the carcinogenicity of iAs due to ROS, as generation of ROS drives epigenetic alterations [5]. The genetic and epigenetic modulation by phytochemicals have been reviewed extensively in the context of carcinogenesis [6]. Tea contains polyphenols and is a good source of antioxidants [7]. Major constituents of black tea are theaflavins (TF) and thearubigins (TR). TF, a seven-member benztropolone ring is formed due to co-oxidation of pairs of epimerized catechins. This molecule is capable of chelating transition metals, thereby countering free

* Corresponding author.
E-mail address: amitava.datta@uwa.edu.au (A. Datta).

https://doi.org/10.1016/j.heliyon.2022.e10341
Received 22 January 2022; Received in revised form 16 March 2022; Accepted 1 August 2022

Table 1. Treatment of different mice groups.

Group	iAs (500 μg/l dissolved in water). Administered orally as only source of water + painted on the shaved hind part, once daily	BTE (0.33 mg/gm body weight, lyophilised extract dissolved in water). Thrice daily by oral gavage
I	No	No
II	Yes	No
III	Yes	Yes

radical generation. Resonance in the benzotropoline moieties quench oxidative species by donating an electron [8]. Of the three main derivatives of TF (theaflavin-3-gallate, theaflavin-3′-gallate, and theaflavin-3-3′-digallate), theaflavin-3-gallate can inhibit the activity of DNA methyltransferase-3a (DNMT3a) by directly binding [9]. Theaflavin-3-3′-digallate can directly interact with model histone proteins, double stranded and quadruplex DNA strands. Therefore, action of TF is due to its translocation to the nucleus and interaction with different nuclear proteins and DNA [9].

Reporting on the influence of iAs on these histone proteins, particularly for SCC of skin in mice model is scanty. The present study aims to investigate the influence of chronic exposure to iAs on the expression of PTM of several histones and their histone methyl transferases (HMT), histone demethylases (HDM) and histone acetyl transferases (HAT) in squamous cell carcinoma and their modulation by BTE. We found that iAs down-regulates H3K4me3 and enhances the level of JARID1B (a H3K4me3 demethylase), while on the other hand, BTE upregulates H3K4me3 but fails to downregulate JARID1B. Based on this finding, we hypothesized that components of BTE may inhibit the demethylation activity of JARID1B. We observed theaflavin and theaflavin-3,3′-digallate dock with high affinity at the JmjC demethylating domain of JARID1B. Molecular dynamical simulations and analyses were performed to validate the stability of these dockings. It is known that theaflavin and theaflavin-3,3′-digallate are transported to the nucleus and interact extensively with histone proteins [9]. JARID1B is a therapeutic target in several cancers and designing small molecule inhibitors for JARID1B is an active research area, and our findings may indicate theaflavin as an effective inhibitor of JARID1B.

2. Methods

2.1. Treatment protocol

4-5 weeks old, male, Swiss albino mice (Mus musculus) were taken from the animal house of Chittaranjan National Cancer Institute (CNCI), with approval from the Institutional Animal Ethics Committee (IAEC 1774/MR- 3/2017/9). Protocols have been followed according to the standard guidelines laid down by the IAEC, certified by CPCSEA (Committee for the Purpose of Control and Supervision of Experiments on Animals), New Delhi. All the mice were handled and experiments done following the ARRIVE protocols.

Mice were fed with synthetic pellets and maintained in alternate 12 h of light and darkness at a temperature of 22 ± 2 °C. All the mice were kept at the same level of the rack, to maintain identical housing condition. Mice were euthanized by an overdose of thiopentone sodium (100 mg/kg body wt).

The animals were divided into three groups, each group consisting of 25 mice, kept in separate cages, each cage harbouring 5 mice (Table 1). Mice were treated with iAs and BTE, doses were based on our previous findings [10]. Arsenic dose was similar to the concentration found in ground water in arsenic-endemic regions [2]. There was a fourth group, which was administered BTE only, where no changes in the parameters were seen, indicating that BTE dose was non-toxic (data not shown). Tissues and blood were collected at different time intervals. Three groups are: I. Control group, was neither administered iAs, nor BTE. Group II mice were exposed to iAs, whereas, group III mice were exposed to iAs and at the same time were fed with BTE. iAs dose was 500 μg/l (arsenite) dissolved in water; administered orally as only source of water, plus painted on the shaved hind part, once daily. Group III were treated with iAs, as in group II, along with BTE (0.33 mg/gm body weight, lyophilised extract dissolved in water), thrice daily by oral gavage, at an interval of 8 h. The groups of mice and their treatment protocols have been summarised in Table 1.

2.2. Preparation and quantification of BTE

2.5% infusion of Black tea was prepared in boiling water and cooled. It was lyophilized in a SCANVAC lyophilizer. The lyophilized product was weighed, reconstituted in water and administered to the mice by gavage (at an interval of 8 h, cumulated dose being 0.33 mg/gm body weight per day) [7]. polyphenolic content of tea was determined by HPLC, which was performed according to the laboratory protocol [11].

HPLC was carried out using a 515 lb dual pump with a control (Waters, USA), a Rheodyne injector, a RP C-18 column by Nova-Pak which was attached to the guard column regulated at 30 °C and a 996 PDA detector (Waters, USA) adjusted to 278 nm. Catechins were separated using gradient of 5–25% acetonitrile in 0.025 M KH_2PO_4, pH 2.4. Isocratic mode was used to separate theaflavin, where the mobile phase consisted of acetic acid: acetone: water in the ratio of 1:60:39 and detected at 365 nm. Integration and calibration of mixture containing catechins and theaflavins were done using the software Millennium 32. The quantification of the content of catechins and theaflavins was done by plotting against the standard.

2.3. Confirmation of skin cancer by histology

The skin tissues collected after sacrificing the mice, were fixed in 10% Neutral Buffered Formalin (NBF). They were then treated with increasing grades of alcohol (50%, 70%, 90% and 100%) and xylene to remove water and fat content respectively. The tissues were then embedded in paraffin and cut into 4 μm thick sections using a microtome (Leica). These tissue sections were stretched on glass slides, stained with haematoxylin and eosin, mounted with DPX and observed under light microscope (Zeiss). The nucleus appeared blue due to haematoxylin staining on a pink background of the cytoplasm, due to counter-staining by eosin. The development of squamous cell carcinoma in the mice skin was confirmed by histology.

2.4. Tumour assessment

The mice were carefully observed for development of skin lesions. Tumours appearing on the skin, >1 mm in diameter were measured periodically using Vernier callipers in all the groups of mice and the mean tumour diameter was calculated. The diameter was then used to obtain the tumour area using the formula (area = πr^2), where r is the radius, i.e., half the diameter.

Developmental stages of Squamous cell carcinoma (SCC) of the skin of mice were confirmed by histological analysis, following standard protocol [12].

2.5. Histone extraction from animal tissues

Histone proteins isolated by acid extraction [13] method. The isolated skin tissues were homogenised in Dounce homogeniser in Triton-X Extraction Buffer (0.5% Triton-X, 2 mM PMSF, 0.02% NaN_3). The mixture was centrifuged at 10,000 rpm for 1 min at 4 °C. The pellet was suspended in extraction buffer (0.5N HCl and 10% glycerol). After centrifugation at 12,000 rpm for 5 min at 4 °C, supernatant was collected and kept overnight with 600μl of acetone at −20 °C. Finally, the pellet after centrifugation at 12,000 rpm was suspended in deionised

water and stored at −80 °C after protein estimation using Bradford's method.

2.6. H3K4 global methylation detection

Global histone methylation was assessed colorimetrically from the isolated histone extracts. EpiQuikTM Global Histone H3K4 Methylation Assay Kit (P-3017-96, Epigentek) was used. The absorbance OD was measured using a microplate reader Tecan infinite-200 PRO, at 450 nm and the methylation (%) was calculated according to the formula: [Methylation % = {OD (Sample–blank)/OD (untreated control–blank)} ×100].

2.7. Western blot analysis

Histone proteins isolated from skin tissues were used to perform the Western blot analysis. 80 μg of protein was loaded into each well and then electrophoresed on SDS-Polyacrylamide gels respectively. Electrophoresis was performed using the buffer (250 mM TRIS, 192 mM glycine, 10% SDS) and separated proteins were electro-transferred to nitrocellulose membranes using transfer buffer (250 mM TRIS, 192 mM glycine, 10% Methanol). After proper Blocking with Bovine Serum Albumin (BSA), membranes were properly washed with Tris Buffered Saline solution (TBS), pH 7.5 (25 mM TRIS HCl and 150 mM NaCl) and then incubated with primary antibodies overnight at 4 °C with constant shaking. The blots were washed 4 times with TBST followed by treatment with either alkaline phosphatase conjugate anti-mouse or anti-rabbit IgG (1:2000 dilutions in TBS) at 4 °C. Membrane was then washed 4 times and incubated with substrate (BCIP/NBT) to visualize the proteins. The Western blot bands were scanned and quantified by using IMAGE MASTER Software (Amersham Pharmacia biosciences, USA).

2.8. Immunohistochemistry

Immunohistochemistry was performed on formalin fixed, paraffin embedded tissues, based on the standard technique [14]. Tissues were incubated overnight with primary antibody at 4 °C, washed with PBS and stained with secondary antibody HRP-conjugated for half an hour at room temperature. It was then stained with diaminobenzidine (DAB), mounted in DPX and observed under microscope. The expressions of various proteins in IHC were analyzed. Minimum of 15 fields at 400x were visualised under a light microscope. The expressions of various proteins in IHC were analyzed using the scoring system as formulated by Allred et al. 1998 [15]. The scoring system classifies the percentage of stained cells into 6 proportion scores (PS) and the intensity of staining into 4 intensity scores (IS). The final Allred score is calculated as the sum of PS and IS. The six categories of PS and four categories of IS are as follows:

Percentage of stained cells	Category of proportion score (PS)
0	0
<1	1
1–10	2
11–33	3
34–66	4
≥67	5

Intensity of staining	Intensity score (IS)
None	0
Weak	1
Intermediate	2
Strong	3

The final Allred Score (AS) is calculated as: PS + IS = AS. The Allred score can be categorized into 9 categories (0–8), the highest score being 8. Each section was scored 5 times and the highest AS was reported.

2.9. Docking

The crystal structure of JARID1B (KDM5B) (PDB ID: 5FUN) was obtained from protein data bank (https://www.rcsb.org). This structure was used for studying small molecule inhibitors for the JmjC domain of JARID1B [16]. The chemical structures of theaflavin (PubChem CID: 135403798) and theaflavin-3,3′-digallate (PubChem CID: 21146795) were downloaded from PubChem (https://pubchem.ncbi.nlm.nih.gov/). Protein and ligand preparations were done using Python Molecular Viewer (pmv), part of MGLTools from Scripps Institute [17].

The PHD1-ARID domains were deleted from JARID1B structure (PDB ID: 5FUN) and it was considered suitable for our study as the focus is on the JmjC domain. Johansson et al. used several supplementary ligands in their study which were removed from the PDB file for molecular dynamical simulations [16]. These supplementary ligands are EDO (1,2 ethanediol), EPE (4-(2-hydroxyethyl)-1-piperazine ethanesulfonic acid), GZA (2-[(1-benzyl-1H-pyrazol-4-yl)oxy]pyrido [3,4-d]pyrimidin-4(3H)-one), metals (Mn, Zn, Na) and phosphate ion. The removal of these supplementary ligands had no effect on the protein structure, which was verified by superimposing the two structures. The protein was prepared by deleting water molecules, adding polar hydrogen and Gasteiger charges, and saved in the pdbqt format. The ligand was prepared by adding Gasteiger charges and saved in the pdbqt format. Docking was done using Webina, a web-based docking tool that runs in a browser using AutoDock Vina [18, 19]. The centre (x = 88, y = 66, z = 11.6) and size (x = 30, y = 27, z = 32) of the docking box were chosen to cover the JmjC domain of JARID1B. The top-9 docking poses for both theaflavin and theaflavin-3,3′-digallate were analyzed for polar interactions using PyMol. The docking poses were extracted from the output using vina_split, a tool in the AutoDock Vina software.

2.10. Molecular dynamical simulation

Preparations of the protein-ligand systems for molecular dynamical simulation were done using Gromacs in-built tools [20] version 2020.1-Ubuntu-2020.1-1 on a 64-bit, quad core Ubuntu system. The Bioexcel Building Block library [https://mmb.irbbarcelona.org/biobb/availability/tutorials/md_setup] workflow was used for preparation of the protein-ligand system, using python 3.7 and Jupyter Notebook. The Amber ff99sb forcefield was used, as this forcefield is considered to be appropriate for protein-ligand simulations. Short (10 ps) molecular dynamical simulations were done at the preparation stage to check the setup parameters.

The Zeus supercomputer in Pawsey Supercomputing Facility in Perth, Western Australia was used for the Gromacs production runs (Intel Xeon E5-2690V3 "Haswell" processors, 12-cores, 2.6 Ghz). 24 MPI processes and 4 OpenMP threads in each MPI process were found to provide optimal performance. Each production simulation was run for 24 h, providing approximately 37 nano seconds of simulation time.

Molecular mechanics Poisson−Boltzmann surface area (MM/PBSA), a widely used method to calculate the binding free energy between protein and ligands was used. Although it is not as accurate as alchemical free energy methods, it is considered to be more accurate than scoring functions used in docking and substantially much faster than the alchemical methods. MM/PBSA analysis was done using the g_mmpbsa tool [21]. The docking movies were created using Gromacs trajectory files.

Table 2. Polyphenolic content of Black Tea Extract (2.5%) Catechins like EGCG [(-)- epigallocatechin gallate, EGC [(-)- epigallocatechin] and ECG [(-)- epicatechin gallate] were separated using gradient mode; while TF [Theaflavin] was separated using isocratic mode.

Polyphenol	Concentration (mg/ml)
EGC	0.24
EGCG	0.43
ECG	0.30
TF	0.97

2.11. Statistical analysis

Statistical analysis was done using Graphpad Prism 8 software. Significance level of $p < 0.001$ was accepted. Comparisons between the groups were done using unpaired t-test.

3. Results

3.1. Polyphenol content of BTE

The polyphenolic contents in BTE were quantitated. Different constituents of Catechins, EGCG [(-)- epigallocatechin gallate, EGC [(-)-epigallocatechin] and ECG [(-)- epicatechin gallate] were separated using gradient mode; whereas TF [Theaflavin] was separated in isocratic mode. Concentrations (mg/ml) are given in Table 2. Theaflavin was found to be the most abundant polyphenolic compound in the BTE extracted which was administered to the mice.

3.2. Development of carcinoma

Schematic representation of the progression of Squamous Cell Carcinoma of the skin has been shown in Figure 1.

Development of SCC of skin by chronic iAs exposure in Swiss albino mice, along with corresponding histology has been depicted in Figure 2. Mice receiving co-treatment of BTE with iAs developed papillomatous lesions, with hyperplasic or mild dysplastic changes, as evident from histology. No cytological atypia or massive infiltration of the dermal layer was observed indicating no development of invasive SCC even at 330 days of treatment.

Minor lesions started appearing in the skin tissues of the iAs treated mice after 90 days of treatment. These lesions further aggravated and developed into major invasive gaping wounds at 330 days. Histopathological analysis of the iAs treated mice revealed the loss of entire epidermal structure and prominent infiltration of the deeply stained, aggressive nuclei, covering more than 2/3rd proportion of the underlying dermis, confirming invasive squamous cell carcinoma.

3.3. Tumour growth dynamics

Lesions started to appear on the shaved skins of the mice of the group II and III after 30 days of treatment. The lesions in the group II mice were visibly larger and more in number covering a larger area of the skin surface, in comparison to the Group III mice which were administered BTE. Figure 3 clearly represents that with chronic exposure of iAs, the diameter (a) and area of the tumours (b) in the iAs treated mice were significantly ($p < 0.0001$) higher than the mice which were administered BTE. The group II mice developed lesions at the 330 days while the lesions of the group III mice were smaller and not that aggressive in appearance. No lesions were observed in the mice of the control group.

3.4. Global methylation status of H3K4

Global methylation status of H3K4 (Figure 4) indicates hypomethylation due to iAs, which can be significantly prevented ($p < 0.0001$) by BTE. Colorimetric estimation of the global methylation status of H3K4 loci revealed a trend of demethylation with chronic iAs exposure. The methylation percentage of H3K4 was significantly low ($p < 0.0001$) in iAs treated group with respect to the control group. The BTE administered mice showed significantly higher ($p < 0.0001$) methylation percentage at 330 days of treatment with respect to the iAs group, indicating inhibition of loss of global methylation at H3K4 loci by BTE.

3.5. Expression of epigenetic histone marks and their modifiers (methyltransferases, demethylases and acetyltransferases)

Western blot analysis reveals alteration in expression of histone modifiers by chronic iAs exposure for 330 days and their modulation by BTE (Figure 5). Significant increase in the expression of H3K4me1, the methyl transferase MLL3, JARID1B, H3K27me3, EZH2 methyltransferase along with JARID2 upon iAs exposure for 330 days was observed. Intervention with BTE in the group of mice exposed to iAs, significantly brought down the elevated expression levels of these proteins due to iAs, though the extent of down-regulation varied. BTE downregulated their

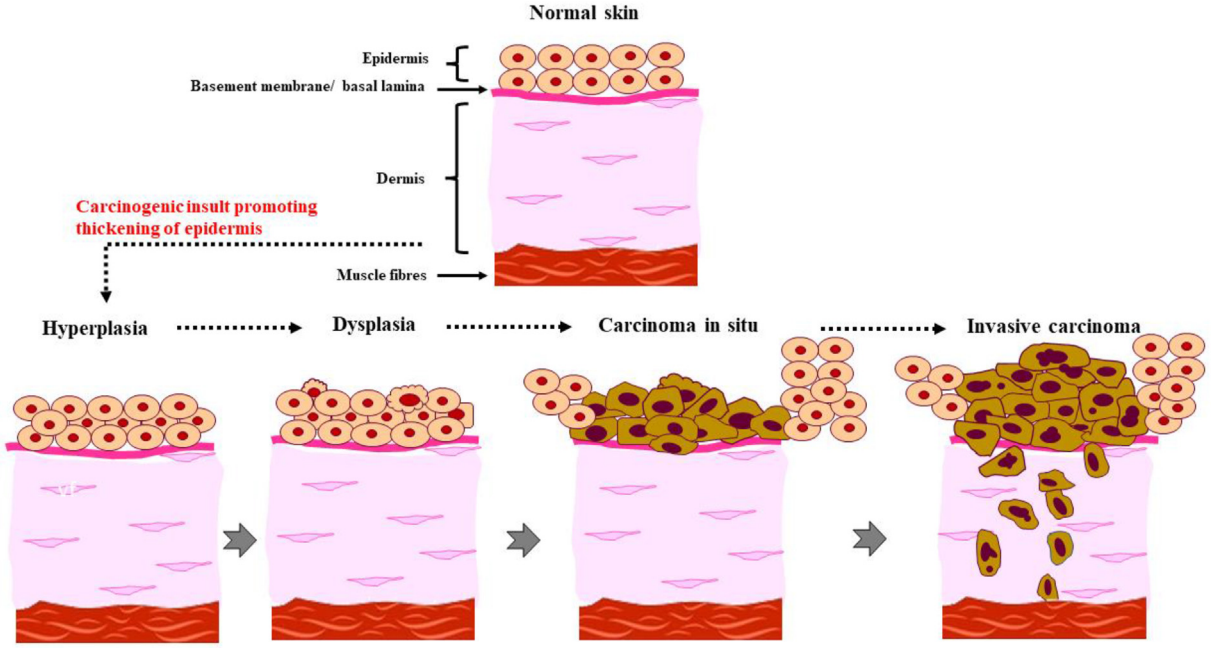

Figure 1. Schematic representation of the development of squamous cell carcinoma of the skin. Carcinogen insult results in thickening of the epidermis and increase in the number of cells, leading to hyperplasia, which may be the initial sign of abnormal or precancerous changes. Hyperplasia may develop into dysplasia, where a number of abnormal cells are seen. These may further promote to localised squamous cell carcinoma (SCC) of the skin, called in situ carcinoma. With passage of time, progression may occur and invasive carcinoma results, where the cancer cells breach the adjacent tissue structure, penetrating and infiltrating it which promotes metastasis and secondary tumour formation.

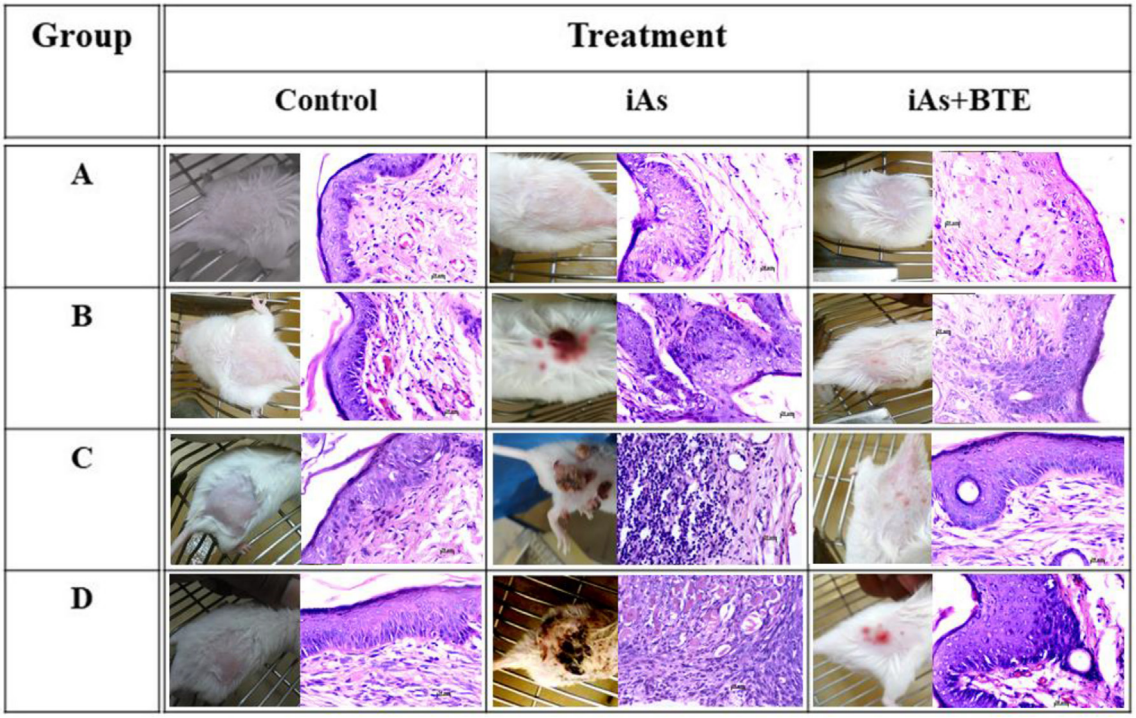

Figure 2. Development of skin carcinoma. Swiss albino mice were chronically exposed to iAs (500 μg/l). Three groups of mice were sacrificed at (A) 30, (B) 180, (C) 270 and (D) 330 days. Histological analysis revealed (A) no visible changes in control and iAs + BTE treated mice; slight thickening of the epidermal layer was observed in iAs group. (B) no changes in control group; in iAs group prominent hyperplasic and dysplastic changes were observed in the epidermal layer; mild hyperplasia was observed in iAs + BTE group. (C) no prominent changes were observed in the epidermal layer of control group; in iAs treated group, formation of in situ carcinoma was observed with regions of the tissue showing loss of epidermal architecture and presence of deeply stained nuclei; whereas, in iAs + BTE group prominent hyperplasic changes were observed with presence of frequent keratin pearls. (D) mild hyperplasic changes were observed in control group, due to aging; in iAs treated group more than two-third of the tissue sections show complete loss of the epidermal architecture, filled with deeply stained nuclei indicating invasive carcinoma; in iAs + BTE, thickening of the epithelium, presence of keratin pearls along with other dysplastic changes were clearly visible in the tissue. Images were captured at 400 x.

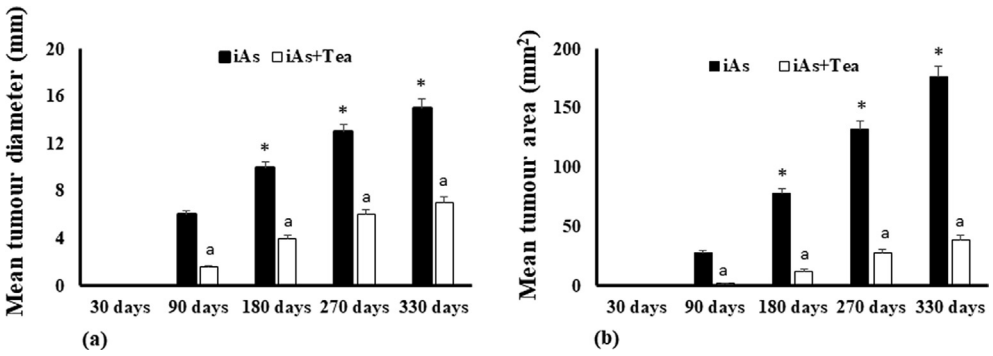

Figure 3. Measurement of tumour size. (a) Tumour diameter has been measured using callipers and the mean value ±SD has been represented as bar diagram at different time points; (b) area of tumour was measured at different time intervals and data has been represented as mean ± SD. There has been no visible tumour at 30 days, therefore, increase in diameter has been calculated with respect to the one obtained at 90 days. Increase in diameter and tumour area are significant (*) at $p < 0.0001$. Intervention with BTE, resulted in appreciable decrease in tumour diameter and area (a), which are significant at $p < 0.0001$, with respect to the group II mice.

over-expression significantly, except for JARID1B, which is not influenced by BTE. Corresponding significance levels are given in Table 3. Contrastingly, chronic exposure to iAs significantly reduced the expression levels of H3K4me3, MLL1, KDM6A, H4K16ac and its acetyltransferase MYST1. Intervention with BTE upregulated the expression of these histone proteins and their modifiers. Expression of demethylase LSD1 however is not influenced either by iAs or iAs + BTE. Corresponding band intensities have been given in Figure 6.

3.6. IHC analysis

Immunohistochemistry of different histone marks and their modifiers have been depicted in Figure 5. Results are in agreement with Western blot analysis. Semi-quantitative assessment of immunostaining results was done using the Allred scoring (AS) system, and the final score for each assessed protein has been shown in Table 4. Allred scoring (AS) for JARID1B showed a significant increase in the iAs treated mice, however, no changes were observed upon BTE administration. H3K4me1, MLL3, JARID1B, EZH2, JARID2, H3K27me3 showed a higher score with respect to those of the control group. The Allred score was found to be diminished in the group of mice with iAs and BTE simultaneously. Lowering of AS in H3K4me3, MLL1, KDM6A, MYST1 and H4K16ac was observed in iAs exposed mice for 330 days. A significant rise in AS score was observed in the group of mice exposed to iAs + BTE regularly. Score for LSD1, a H3K4me2/me1 demethylase remained unchanged by iAs, but a slight reduction in score was observed in iAs + BTE group. But, this reduction in LSD1 level was not significant.

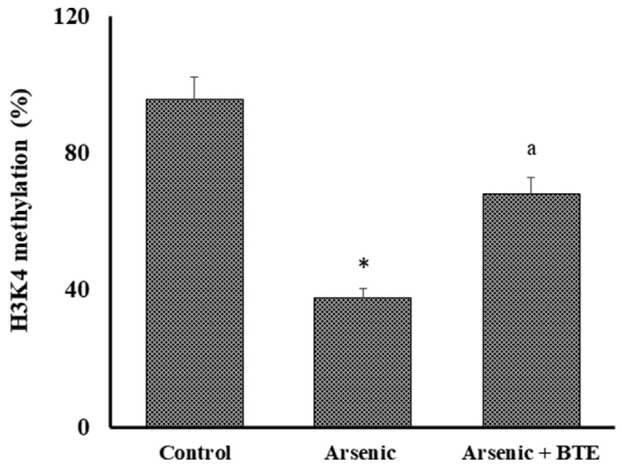

Figure 4. Global methylation at H3K4 loci. Global methylation has been depleted to 0.4-fold by exposure to iAs for 330 days. Reduced methylation at H3K4 loci has been increased by BTE administration. Values are average of three independent experiments ±SD. Reduction in global H3K4 methylation is significant with respect to control at $p < 0.0001$; enhancement of the same by BTE is significant at $p < 0.0001$.

3.7. In silico docking studies

Initial docking of JARID1B and theaflavin was done in the presence of the supplementary ligands with high docking affinity. Fe(II) ion was replaced by Mn(II) ion [16], and several C and H atoms of theaflavin were docked less than 2 Å from the Mn(II) ion. Both theaflavin and theaflavin-3,3′-digallate were docked after removing the supplementary ligands. The structure of JARID1B (PDB id: 5FUN) downloaded from PDB with additional ligands and the corresponding cleaned structure of the same are shown in Figure 7. Both theaflavin and theaflavin-3,3′-digallate were docked after removing the supplementary ligands (Figure 7), with high affinities (−9.7 kCal/mole and −11.5 kCal/mole respectively). Top two poses of cleaned protein docked with theaflavin and theaflavin-3,3′-digallate are shown in Figure 5. Analysis using PyMol showed at least one hydrogen bond and several medium range (<10 Å) polar interactions. Two beta sheets each from either side of the JmjC domain were within 5 Å distance from the docked ligands (theaflavin and theaflavin-3,3′-digallate).

3.8. Molecular dynamical simulation

MM/PBSA calculations were done on the trajectories of the systems between 30-31 ns from the production run. The time evolution of the RMSDs shows the systems to be fairly stabilized during this period. The lower the calculated binding energy, the stronger the ligand is expected to bind to the protein. From our calculations (Figure 7) it appears that the binding affinity of theaflavin-3,3′-digallate for the JmjC domain of JARID1B is higher than theaflavin.

Time evolution and variation in different energy components as observed from molecular dynamical simulations of JARID1B with theaflavin-3,3′-digallate for the top docking pose are shown in Figure 8. We chose to include the results for the top docking pose of theaflavin-3,3′-digallate due to its higher affinity for docking with JARID1B. The protein-ligand trajectories for the top poses of theaflavin and theaflavin-3,3′-digallate are shown in videos: https://bit.ly/3oObA4s for theaflavin and https://bit.ly/2YzLSWK for theaflavin-3,3′-digallate.

4. Discussion

Invasive SCC of skin was observed at 330 days of iAs treatment. With BTE intervention, only hyperplasic and dysplastic changes were

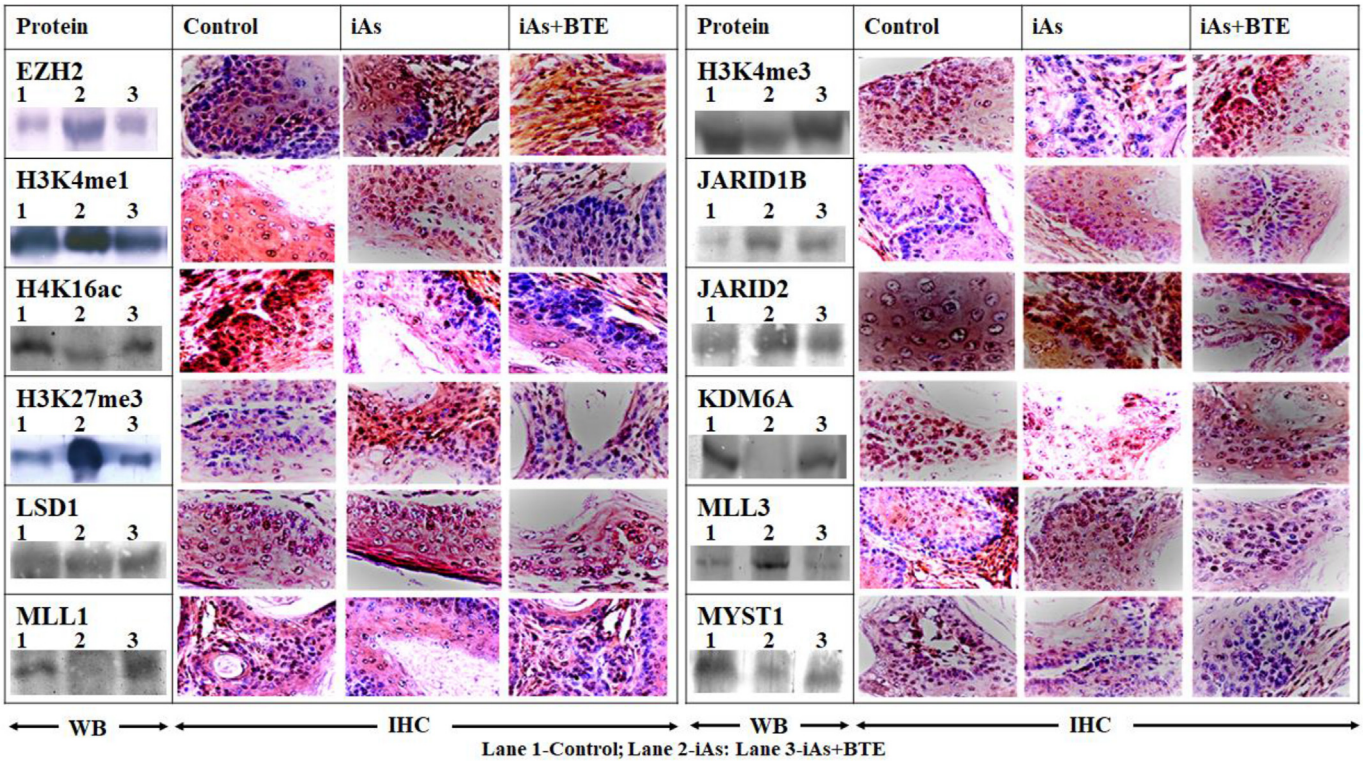

Figure 5. Influence of iAs on the expression of epigenetic histone marks and their modifiers (methyltransferases, demethylases and acetyltransferases). Western blot bands and corresponding IHC results from skin tissue of mice after 330 days of exposure using corresponding antibodies have been depicted. In Western blot bands, Lanes 1, 2, 3 represent control, iAs and iAs + BTE treated mice respectively. In IHC, formalin fixed, paraffin embedded section of skin tissues after incubation with primary antibody were stained with DAB. Images were captured at 400 x.

Table 3. Modulation of Histone marks with significance levels.

	Significance (p value)			
	Western blot band intensity		Allred score (IHC)	
	Expression level after iAs, wrt control	Expression level after intervention with BTE, wrt iAs exposure	Score after iAs, wrt control	Score after intervention with BTE, wrt iAs exposure
PLU1/JARID1B	↓$p < 0.0001$	$p = 0.6787$	↓$p < 0.0001$	$p = 0.1442$
JARID2	↓$p < 0.0001$	↓$p < 0.005$	↓$p < 0.0001$	↓$p < 0.005$
EZH2	↓$p < 0.0001$	↓$p < 0.005$	↓$p < 0.0001$	↓$p < 0.0001$
LSD1	$p = 0.4199$	$p = 0.3000$	$p = 1.000$	$p = 0.0847$
H3K4me1	↓$p < 0.005$	↓$p < 0.005$	↓$p < 0.0001$	↓$p < 0.005$
H3K4me3	↓$p < 0.0001$	↓$p < 0.005$	↓$p < 0.0001$	↓$p < 0.0001$
MLL1	↓$p < 0.0001$	↓$p < 0.005$	↓$p < 0.0001$	↓$p < 0.005$
MLL3	↓$p < 0.0001$	↓$p < 0.005$	↓$p < 0.005$	↓$p < 0.005$
KDM6A	↓$p < 0.0001$	↓$p < 0.005$	↓$p < 0.0001$	↓$p < 0.005$
MYST1	↓$p < 0.0001$	↓$p < 0.005$	↓$p < 0.0001$	↓$p < 0.0001$
H4K16ac	↓$p < 0.0001$	↓$p < 0.005$	↓$p < 0.0001$	↓$p < 0.005$
H3K27me3	↓$p < 0.0001$	↓$p < 0.0001$	↓$p < 0.0001$	↓$p < 0.0001$

Statistical analysis was done using Graphpad Prism 8 software. Significance level of $p<0.001$ was accepted. Comparisons between the groups were done using unpaired t-test.

observed, where epidermal architecture of the tissue remained mostly intact with the absence of major invasive structures within the dermal layer. PTMs of histones are prognostic cancer markers [22] and our study focuses on the PTMs of three histone loci, namely H4K16, H3K27 and H3K4, as well as several histone methylases, demethylases and acetyltransferases.

H4K16ac and its acetyltransferase MYST1, have been found to be associated with the promoters of actively transcribed genes. Silencing of MYST1 by iAs reduces H4K16ac, which is involved in DNA damage response [23]. In our study, development of invasive SCC due to iAs, may be partly due to loss of H4K16ac and MYST1. H4K16ac is downregulated in some cancers, e.g., renal cell carcinoma, medulloblastoma, breast cancer, colorectal cancer [24, 26] and ovarian cancer [25]; and upregulated in non-small cell lung carcinoma [24]. Significant upregulation of MYST1 has been reported recently in glioblastoma [27]. Prevention of invasive SCC by BTE may be partially attributed to the upregulation of H4K16ac and MYST1.

H3K27me3 is involved in transcriptional silencing [28] and is upregulated in several cancers. H3K27me3, a prognostic marker in various cancers, exhibits negative correlation with patient survival rates [29], as well as modulates oncogenes, tumor suppressor genes, cell cycle regulatory and cell adhesion genes in gastric cancer [30]. Methyl transferase EZH2 promotes methylation of H3K27me3 via the PRC2 complex [28]. EZH2 is significantly overexpressed in prostate cancer, resulting in excessive methylation of H3K27me3 and silencing of several key tumor suppressor genes [31, 32]. Upregulation of EZH2 was reported in breast and ovarian cancer, while its inhibition has shown to promote apoptosis via H3K27me3 reduction [33]. JARID2, an important component of this complex, plays a pivotal role in its methylation and gene silencing activity [28]. KDM6A, a H3K27me3 demethylase, has been reported to exhibit tumor suppressive role in squamous-like pancreatic cancer [34].

The present study reports an increase of H3K27me3 along with EZH2 and JARID2, suggesting an active role of the PRC2 complex. Suppression of KDM6A by chronic exposure to iAs may promote SCC of skin, which may be prevented by BTE. Anomalously, studies in human lung

Table 4. Allred Score for IHC of epigenetic markers.

Proteins	Control	Arsenic (iAs)	iAs + BTE
PLU1/JARID1B	4 ± 0.63	6 ± 0.63*	6 ± 0.91
JARID2	5 ± 0.45	7 ± 0.31*	6 ± 0.45[b]
EZH2	4 ± 0.44	8 ± 0.21*	6 ± 0.45[a]
LSD1	6 ± 0.45	6 ± 0.55	5 ± 0.62
H3K4me1	5 ± 0.45	7 ± 0.38*	6 ± 0.32[b]
H3K4me3	7 ± 0.38	4 ± 0.45*	6 ± 0.45[a]
MLL1	7 ± 0.45	5 ± 0.50*	6 ± 0.32[b]
MLL3	6 ± 0.45	7 ± 0.45**	6 ± 0.38[b]
KDM6A	7 ± 0.45	5 ± 0.50*	6 ± 0.21[b]
MYST1	7 ± 0.45	4 ± 0.50*	6 ± 0.50[a]
H4K16ac	7 ± 0.45	4 ± 0.50*	5 ± 0.32[b]
H3K27me3	4 ± 0.54	8 ± 0.21*	6 ± 0.45[a]

The Allred score (AS) of the respective immunoblotted proteins of the different treatments of mice have been tabulated
Significant at *$p < 0.0001$, **$p < 0.005$ with respect to control group.
Significant at [a] $p < 0.0001$, [b] $p < 0.005$ with respect to iAs group.

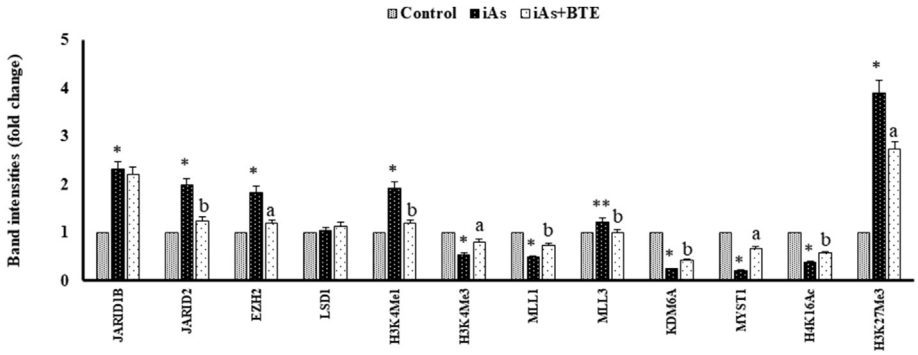

Figure 6. Modulation of various histone marks by iAs during skin carcinogenesis, as modulated by BTE. Band intensities (fold change) as obtained from Western blot results (from Figure 5) have been represented in a bar diagram. Values are the mean band intensities of three independent experiments ±SD. Modulation of histone marks induced by iAs with respect to control is significant, *$p < 0.0001$; **$p < 0.005$. Reversal of aberrant histone marks by BTE with respect to iAs group are significant at [a]$p<0.0001$, [b]$p<0.005$.

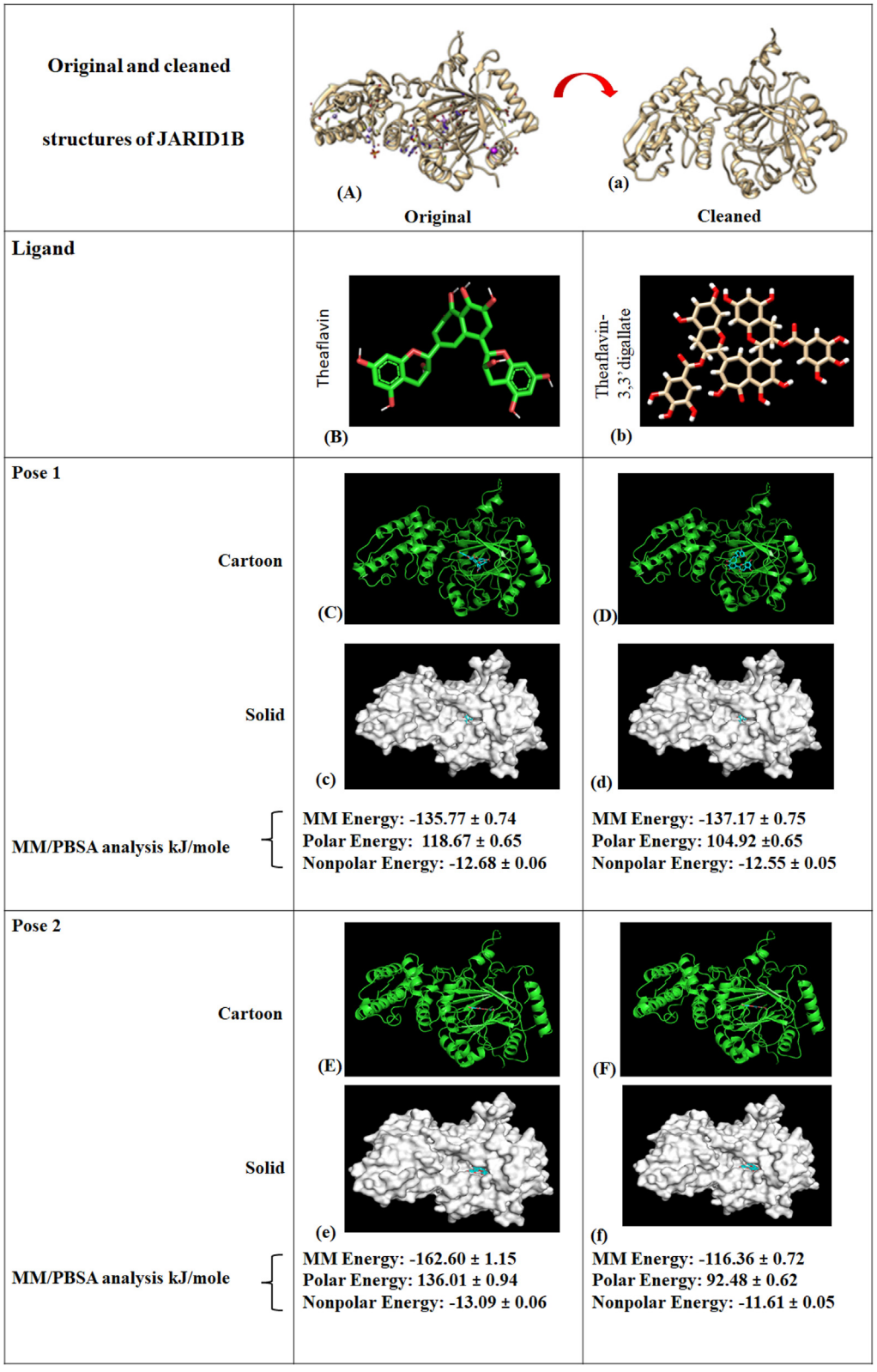

Figure 7. Docking results of JARID1B. (A) The original structure of JARID1B (PDB id: 5FUN) downloaded from PDB with additional ligands; (a) The cleaned structure of JARID1B (PDB id: 5FUN) downloaded from PDB with additional ligands; (B) Chemical structure of theaflavin; (b) Chemical structure of theaflavin-3,3′-digallate; (C) The best docking pose of theaflavin with JARID 1B (cartoon rendering); (c) The best docking pose of theaflavin with JARID 1B (solid rendering); (D) The best docking pose of theaflavin-3,3′-digallate with JARID 1B (cartoon rendering); (d) The best docking pose of theaflavin-3,3′-digallate with JARID 1B (solid rendering). (E) The 2nd best docking pose of theaflavin with JARID 1B (cartoon rendering); (e) The 2nd best docking pose of theaflavin with JARID 1B (solid rendering); (F) The 2nd best docking pose of theaflavin-3,3′-digallate with JARID 1B (cartoon rendering); (f) The 2nd best docking pose of theaflavin-3,3′-digallate with JARID 1B (solid rendering). The corresponding MM/PBSA analyses results have been shown below the figures.

carcinoma cell line A459 showed a repression of H3K27me3 upon iAs exposure [35]. ROS generation also promotes H3K27me3 overexpression [36].

H3K4 loci has three methylation states, H3K4me1/2/3, which are associated with promoters of the active genes and temporarily stalled genes [37]. In our study, higher expressions of H3K4me1 and MLL3 (the methyltransferase for H3K4me1) were observed in mice having invasive SCC due to iAs; this may be due to the formation of oncogenic super-enhancers, aggregation of 700–1300 bases of H3K4me1 and H3K27ac at the promoter regions of genes [37]. MLL3 promotes mono-methylation of H3K4, indirectly inducing oncogenic super-enhancer formation [38]. Anomalously, suppression of MLL3

expression due to a mutation has been implicated in growth of colorectal cancer cells [39].

Methyl transferase MLL1 plays an important role in methylation of H3K4 loci including its trimethylation [40]. LSD1 demethylates H3K4me1/2 in breast and prostate cancer while its inhibition upregulates tumor suppressor activity [41]. Our data reveals downregulation of H3K4me3 and MLL1 in the iAs treated mice. However, in the present study LSD1 did not show any modulation due to BTE. Loss of both H3K4me3 and MLL1 may cause silencing of the tumor suppressor genes and promotion of carcinogenesis [37]. BTE enhances the expression of H3K4me3 and MLL1. This may promote tumor suppressing activity. Abnormally high H3K4me3 (500–3500 bps), an epigenetic signature 'Broad H3K4me3' is present in the promoters of tumor suppressor genes or cell identity genes, lowering of which has been reported in cancer cells [37]. iAs exposure has shown overexpression of H3K4me3 in lung cancer cell line [35]. It also modulates histone methyl transferases and demethylases altering global expression of H3K4me3 [42]. Anomalously, it has been reported that anti-PD-L1 or anti-PD-1 antibody immunotherapy in combination with, inhibition of MLL1 suppresses pancreatic tumor growth [43].

According to a study, ROS generation led to H3K4me3 overexpression [36]. Repressed H3K4Me2/3 correlates with low grade carcinoma and high recurrence of prostate, breast, pancreatic, renal and non-small cell carcinoma [44, 45, 46, 47]. JARID1B, a H3K4me3 demethylase, was found to be upregulated by iAs with a concomitant downregulation of H3K4me3, showing its demethylating activity. High expression of JARID1B has been reported in human hypopharyngeal squamous cell carcinoma [48], metastatic triple negative breast cancer [49], colorectal cancer [50], prostate cancer, lung cancer, ER + breast cancer, osteosarcoma, melanoma, glioma, oral cancers, gastric cancer, hepatocellular carcinoma and pancreatic cancer [51, 52]. Suppression of JARID1B may halt epithelial to mesenchymal transition via upregulation of E-cadherin, thereby preventing carcinogenesis [53]. Our findings show that BTE failed to downregulate the iAs induced elevated level of JARID1B, though prominent upregulation of H3K4me3 was observed due to the administration of BTE.

High concentration of JARID1B in cancer stem cells (CSC) expressed oral CSC markers including CD44 and ALDH1 and showed increased PI3K pathway activation [54]. Elevated levels of JARID1B expression were observed in over 87% of head and neck squamous cell carcinoma cases [55]. We hypothesized that elevation of H3K4me3 by BTE may be due to inhibition of JARID1B, without any impact on its expression. For a better understanding of this phenomenon, in-silico studies (docking) with JARID1B and the active molecules in black tea were undertaken.

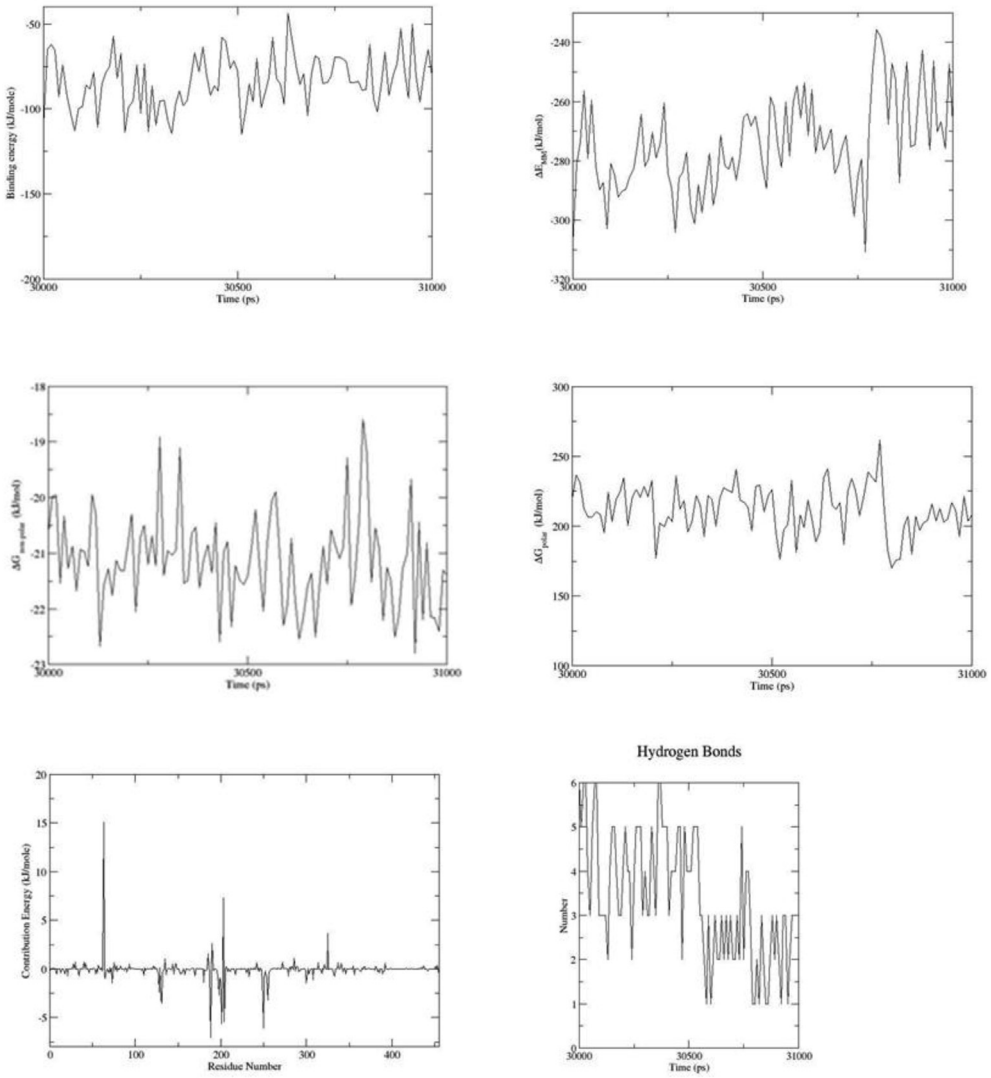

Figure 8. Analysis of different energy values for the binding of the top pose of theaflavin-3,3′-digallate with JARID1B between 30-31 ns of Gromacs simulation. (a) total binding energy-low total binding energy indicates stable docking; (b) MM energy; (c) non-polar binding energy; (d) polar binding energy; (e) per residue binding energy; (f) hydrogen bonds–the graph shows up to 6 hydrogen bonds, and at least 1 hydrogen bond during the simulation period between 30-31 ns.

Results show that both theaflavin and theaflavin-3,3′-digallate dock with high affinity with JARID1B. As the Fe(II) ion is crucial for the demethylation activity of the JmjC domain, theaflavin may have inhibitory effects on the Fe(II) ion, as it docked very close to the Mn(II) that replaced Fe(II) in the crystal structure.

The exact role of the JmjC domain in substrate recognition and binding is still not completely understood, however, our results show that both theaflavin and theaflavin-3,3′-digallate dock in the JmjC domain with high affinity. It has been reported that both these molecules are transported to the nucleus and interact extensively with histone proteins [9] hence it is possible that BTE inhibits JARID1B from its demethylation activity due to theaflavin compounds docking at the JmjC domain.

High affinity in docking results does not always prove good protein-ligand docking [56]. Molecular dynamical (MD) simulation is important to analyse the stability of docking, and also to check whether there are significant differences in the docked poses when MD simulations are run for tens of nanoseconds [56]. We did MM-PBSA analysis on Gromacs trajectories to verify the stability of docking. The trajectories of both theaflavin and theaflavin-3,3′-digallate show that the initial poses are maintained after 30 ns of simulation time.

Chronic exposure of iAs in Swiss albino mice resulted in invasive SCC, while no such carcinogenic development was observed in BTE administered mice. iAs, through modulation of certain HMTs, HDMs and HATs, altered repressive and activating histone marks like H3K27me3, H3K4me1, H3K4me3 and H4K16ac respectively. On the other hand, BTE, showed efficacy in modulating these markers, eliciting its chemopreventive role.

Declarations

Author contribution statement

Madhumita Roy: Conceived and designed the experiments; Contributed reagents, materials, analysis tools or data; Wrote the paper. Archismaan Ghosh: Performed the experiments; Wrote the paper. Amitava Datta: Analyzed and interpreted the data; Wrote the paper. Ansuman Lahiri & Sutapa Mukherjee: Analyzed and interpreted the data.

Data availability statement

Data associated with this study has been deposited at: doi: 10.6084/m9.figshare.c.5794907.

Declaration of interest's statement

The authors declare no conflict of interest.

Additional information

Supplementary content related to this article has been published online at https://doi.org/10.1016/j.heliyon.2022.e10341.

Acknowledgements

The authors are indebted to Director, Chittaranjan National Cancer Institute (CNCI) Kolkata, INDIA, for providing financial and infrastructural support.

References

[1] C.G. Howe, M.V. Gamble, Influence of arsenic on global levels of histone posttranslational modifications: a review of the literature and challenges in the field, Curr. Environ. Health Rep. 3 (2016) 225–237.
[2] M. Roy, D. Sinha, S. Mukherjee, J. Biswas, Curcumin prevents DNA damage and enhances the repair potential in a chronically arsenic-exposed human population in West Bengal, India, Eur. J. Cancer Prev 20 (2011) 123–131.
[3] J.Y. Chung, S.D. Yu, Y.S. Hong, Environmental source of arsenic exposure, J. Prev. Med. Public Health 47 (2014) 253–257.
[4] P. Bhattacharjee, S. Paul, P. Bhattacharjee, Understanding the mechanistic insight of arsenic exposure and decoding the histone cipher, Toxicology 430 (2020), 152340.
[5] Carlos-Reyes Á, J.S. López-González, M. Meneses-Flores, D. Gallardo-Rincón, E. Ruíz-García, L.A. Marchat, et al., Dietary compounds as epigenetic modulating agents in cancer, Front. Genet. 10 (2019) 79.
[6] M. Roy, A. Datta, Cancer Genetics and Therapeutics - Focus on Phytochemicals, first ed., Springer, Singapore, 2019.
[7] D. Sinha, S. Roy, M. Roy, Antioxidant potential of tea reduces arsenite induced oxidative stress in Swiss albino mice, Food Chem. Toxicol 48 (2010) 1032–1039.
[8] Y.Y. Wu, W. Li, Y. Xu, E.H. Jin, Y.Y. Tu, Evaluation of the antioxidant effects of four main theaflavin derivatives through chemiluminescence and DNA damage analyses, J. Zhejiang Univ. - Sci. B 12 (2011) 744–751.
[9] G. Mikutis, H. Karaköse, R. Jaiswal, A. LeGresley, T. Islam, M. Fernandez-Lahore, et al., Phenolic promiscuity in the cell nucleus–epigallocatechingallate (EGCG) and theaflavin-3,3'-digallate from green and black tea bind to model cell nuclear structures including histone proteins, double stranded DNA and telomeric quadruplex DNA, Food Funct 4 (2013) 328–337.
[10] A. Ghosh, S. Mukherjee, M. Roy, Chemopreventive role of black tea extract in Swiss albino mice exposed to inorganic arsenic, Asian Pac. J. Cancer Prev. APJCP 22 (2021a) 647–3661.
[11] D. Sinha, M. Roy, S. Dey, M. Siddiqi, R.K. Bhattacharya, Modulation of arsenic induced cytotoxicity by tea, Asian Pac. J. Cancer Prev. APJCP 4 (2003) 233–237. PMID: 14507244.
[12] A.K. Jain, N. Tewari-Singh, S. Inturi, D.J. Orlicky, C.W. White, R. Agarwal, Histopathological and immunohistochemical evaluation of nitrogen mustard-induced cutaneous effects in SKH-1 hairless and C57BL/6 mice, Exp. Toxicol. Pathol. 66 (2014) 129–138.
[13] D. Shechter, H.L. Dormann, C.D. Allis, S.B. Hake, Extraction, purification and analysis of histones, Nat. Protoc. 2 (2007) 1445–1457.
[14] T. Hashimoto, M. Yamakawa, S. Kimura, O. Usuba, M. Toyono, Expression of acetylated and dimethylated histone H3 in colorectal cancer, Dig. Surg. 30 (2013) 249–258.
[15] D.C. Allred, J.M. Harvey, M. Berardo, G.M. Clark, Prognostic and predictive factors in breast cancer by immunohistochemical analysis, Mod. Pathol. 11 (1998) 155–168. PMID: 9504686.
[16] C. Johansson, S. Velupillai, A. Tumber, A. Szykowska, E.S. Hookway, R.P. Nowak, et al., Structural analysis of human KDM5B guides histone demethylase inhibitor development, Nat. Chem. Biol. 12 (2016) 539–545.
[17] M.F. Sanner, Python: a programming language for software integration and development, J. Mol. Graph. Model. 17 (1999) 57–61. PMID: 10660911.
[18] O. Trott, A.J. Olson, AutoDock Vina: improving the speed and accuracy of docking with a new scoring function, efficient optimization and multithreading, J. Comput. Chem. 31 (2010) 455–461.
[19] Y. Kochnev, E. Hellemann, K.C. Cassidy, J.D. Durrant, Webina: an open-source library and web app that runs AutoDock Vina entirely in the web browser, Bioinformatics 36 (2020) 4513–4515.
[20] M.J. Abraham, T. Murtola, R. Schulz, S. Páll, J.C. Smith, B. Hess, et al., GROMACS: high performance molecular simulations through multi-level parallelism from laptops to supercomputers, Software 1–2 (2015) 19–25.
[21] R. Kumari, R. Kumar, A. Lynn, g_mmpbsa- A GROMACS tool for high-throughput MM-PBSA calculations, J. Chem. Inf. Model. 54 (2014) 1951–1962.
[22] S.A. Khan, D. Reddy, S. Gupta, Global histone post-translational modifications and cancer: biomarkers for diagnosis, prognosis and treatment? World J. Biol. Chem. 6 (2015) 333–345.
[23] K.M. Miller, S.P. Jackson, Histone marks: repairing DNA breaks within the context of chromatin, Biochem. Soc. Trans. 40 (2012) 370–376.
[24] D. Wu, Y. Qiu, Y. Jiao, Z. Qiu, D. Liu, Small molecules targeting HATs, HDACs, and BRDs in cancer therapy, Front. Oncol. 10 (2020), 560487.
[25] N. Liu, R. Zhang, X. Zhao, J. Su, X. Bian, J. Ni, et al., A potential diagnostic marker for ovarian cancer: involvement of the histone acetyltransferase, human males absent on the first, Oncol. Lett. 6 (2013) 393–400.
[26] A. Ghosh, S. Mukherjee, M. Roy, A. Datta, Modulatory role of tea in arsenic induced epigenetic alterations in carcinogenesis, Nucleus 64 (2021b) 143–156.
[27] Z. Dong, J. Zou, J. Li, Y. Pang, Y. Liu, C. Deng, et al., MYST1/KAT8 contributes to tumor progression by activating EGFR signaling in glioblastoma cells, Cancer Med 8 (2019) 7793–7808.
[28] S. Sanulli, N. Justin, A. Teissandier, K. Ancelin, M. Portoso, M. Caron, et al., JARID2 methylation via the PRC2 complex regulates H3K27me3 deposition during cell differentiation, Mol. Cell 57 (2015) 769–783.
[29] C. Tzao, H.J. Tung, J.S. Jin, G.H. Sun, H.S. Hsu, B.H. Chen, et al., Prognostic significance of global histone modifications in resected squamous cell carcinoma of the esophagus, Mod. Pathol. 22 (2009) 252–260.
[30] L. Zhang, K. Zhong, Y. Dai, H. Zhou, Genome-wide analysis of histone H3 lysine 27 trimethylation by ChIP-chip in gastric cancer patients, J. Gastroenterol. 44 (2009) 305–312.
[31] S. Varambally, S.M. Dhanasekaran, M. Zhou, T.R. Barrette, C.K. Sinha, M.G. Sanda, et al., The polycomb group protein EZH2 is involved in progression of prostate cancer, Nature 419 (6907) (2002) 624–629.
[32] M. Ngollo, A. Lebert, M. Daures, G. Judes, K. Rifai, L. Dubois, et al., Global analysis of H3K27me3 as an epigenetic marker in prostate cancer progression, BMC Cancer 17 (2017) 261.
[33] L. Gan, Y. Yang, Q. Li, Y. Feng, T. Liu, W. Guo, et al., Epigenetic regulation of cancer progression by EZH2: from biological insights to therapeutic potential, Biomark Res 6 (2018) 10.

[34] J. Andricovich, S. Perkail, Y. Kai, N. Casasanta, W. Peng, A. Tzatsos, Loss of KDM6A activates super-enhancers to induce gender-specific squamous-like pancreatic cancer and confers sensitivity to BET inhibitors, Cancer Cell 33 (2018) 512–526.
[35] X. Zhou, H. Sun, T.P. Ellen, H. Chen, M. Costa, Arsenite alters global histone H3 methylation, Carcinogenesis 29 (2008) 1831–1836.
[36] Y. Niu, T.L. Desmarais, Z. Tong, Y. Yao, M. Costa, Oxidative stress alters global histone modification and DNA methylation, Free Radic. Biol. Med. 82 (2015) 22–28.
[37] S.S. Dhar, D. Zhao, T. Lin, B. Gu, K. Pal, S.J. Wu, et al., MLL4 is required to maintain broad H3K4me3 peaks and super-enhancers at tumor suppressor genes, Mol. Cell 70 (2018) 825–841.
[38] Q. Jia, S. Chen, Y. Tan, Y. Li, F. Tang, Oncogenic super-enhancer formation in tumorigenesis and its molecular mechanisms, Exp. Mol. Med. 52 (2020) 713–723.
[39] C. Larsson, L. Cordeddu, L. Siggens, T. Pandzic, S. Kundu, L. He, et al., Restoration of KMT2C/MLL3 in human colorectal cancer cells reinforces genome-wide H3K4me1 profiles and influences cell growth and gene expression, Clin. Epigenet. 12 (2020) 74.
[40] Y. Fang, D. Zhang, T. Hu, H. Zhao, X. Zhao, Z. Lou, et al., KMT2A histone methyltransferase contributes to colorectal cancer development by promoting cathepsin Z transcriptional activation, Cancer Med 8 (2019) 3544–3552.
[41] S. Lim, A. Janzer, A. Becker, A. Zimmer, R. Schüle, R. Buettner, et al., Lysine-specific demethylase 1 (LSD1) is highly expressed in ER-negative breast cancers and a biomarker predicting aggressive biology, Carcinogenesis 31 (2010) 512–520.
[42] W. Tu, Y. Liu, C. Xie, X. Zhou, Arsenite downregulates H3K4 trimethylation and H3K9 dimethylation during transformation of human bronchial epithelial cells, J. Appl. Toxicol. 38 (2018) 480–488.
[43] C. Lu, A.V. Paschall, H. Shi, N. Savage, J.L. Waller, M.E. Sabbatini, et al., The MLL1-H3K4me3 axis-mediated PD-L1 expression and pancreatic cancer immune evasion, J. Natl. Cancer Inst. 109 (2017) 283.
[44] F. Barlési, G. Giaccone, M.I. Gallegos-Ruiz, A. Loundou, S.W. Span, P. Lefesvre, et al., Global histone modifications predict prognosis of resected non-small-cell lung cancer, J. Clin. Oncol. 25 (2007) 4358–4364.
[45] S.E. Elsheikh, A.R. Green, E.A. Rakha, D.G. Powe, R.A. Ahmed, H.M. Collins, et al., Global histone modifications in breast cancer correlate with tumor phenotypes, prognostic factors, and patient outcome, Cancer Res 69 (2009) 3802–3809.
[46] J. Ellinger, P. Kahl, C. Mertens, S. Rogenhofer, S. Hauser, W. Hartmann, et al., Prognostic relevance of global histone H3 lysine 4 (H3K4) methylation in renal cell carcinoma, Int. J. Cancer 127 (2010) 2360–2366.
[47] A. Manuyakorn, R. Paulus, J. Farrell, N.A. Dawson, S. Tze, G. Cheung-Lau, et al., Cellular histone modification patterns predict prognosis and treatment response in resectable pancreatic adenocarcinoma: results from RTOG 9704, J. Clin. Oncol. 28 (2010) 1358–1365.
[48] J. Zhang, X. An, Y. Han, R. Ma, K. Yang, L. Zhang, et al., Overexpression of JARID1B promotes differentiation via SHIP1/AKT signaling in human hypopharyngeal squamous cell carcinoma, Cell Death Dis 7 (2016) e2358.
[49] O.A. Bamodu, W.C. Huang, W.H. Lee, A. Wu, L.S. Wang, M. Hsiao, et al., Aberrant KDM5B expression promotes aggressive breast cancer through MALAT1 overexpression and downregulation of hsa-miR-448, BMC Cancer 16 (2016) 160.
[50] D. Huang, F. Xiao, H. Hao, F. Hua, Z. Luo, Z. Huang, et al., JARID1B promotes colorectal cancer proliferation and Wnt/β-catenin signaling via decreasing CDX2 level, Cell Commun. Signal 18 (2020) 169.
[51] J. Taylor-Papadimitriou, J. Burchell, JARID1/KDM5 demethylases as cancer targets? Expert Opin. Ther. Targets 21 (2017) 5–7.
[52] L.H. Kristensen, A.L. Nielsen, C. Helgstrand, M. Lees, P. Cloos, J.S. Kastrup, et al., Studies of H3K4me3 demethylation by KDM5B/Jarid1B/PLU1 reveals strong substrate recognition in vitro and identifies 2,4-pyridine-dicarboxylic acid as an in vitro and in cell inhibitor, FEBS J 279 (2012) 1905–1914.
[53] B. Tang, G. Qi, F. Tang, S. Yuan, Z. Wang, X. Liang, et al., JARID1B promotes metastasis and epithelial-mesenchymal transition via PTEN/AKT signaling in hepatocellular carcinoma cells, Oncotarget 6 (2015) 12723–12739.
[54] N.D. Facompre, K.M. Harmeyer, X. Sole, S. Kabraji, Z. Belden, V. Sahu, et al., JARID1B enables transit between distinct states of the stem-like cell population in oral cancers, Cancer Res 76 (2016) 5538–5549.
[55] Z. Cui, L. Song, Z. Hou, Y. Han, Y. Hu, Y. Wu, et al., PLU-1/JARID1B overexpression predicts proliferation properties in head and neck squamous cell carcinoma, Oncol. Rep. 33 (2015) 2454–2460.
[56] Y.C. Chen, Beware of docking, Trends Pharmacol. Sci. 36 (2015) 78–95.